International Journal of Engineering and Geosciences (IJEG),
Vol; 4, Issue; 3, pp. 149-156, October, 2019, ISSN 2548-0960, Turkey,
DOI: 10.26833/ijeg.549944

LAND SURFACE TEMPERATURE ANOMALIES IN RESPONSE TO CHANGES IN FOREST COVER

Behnam Khorrami [1*], Orhan Gunduz [2], Nilanchal Patel [3], Souad Ghouzlane [4], Mohamed Najar [5]

[1,4,5] Dokuz Eylul University, The Graduate School of Natural and Applied Sciences, Department of GIS, Izmir, Turkey (Behnam.Khorrami/Mohamed.Najar@ogr.deu.edu.tr,); **ORCID 0000-0003-3265-372X, 0000-0002-9107-961X.** (souad.ghouzlane@gmail.com), **ORCID 0000-0001-5781-5874**

[2] Dokuz Eylul University, Faculty of Engineering, Department of Environmental Engineering Izmir, Turkey (orhan.gunduz@deu.edu.tr); **ORCID 0000-0001-6302-0277**

[3] Birla Institute of Technology Mesra, Department of Remote Sensing, Ranchi, India (npatel@bitmesra.ac.in); **ORCID 0000-0003-1011-8419**

*Corresponding Author, Received: 05/04/2019, Accepted: 12/07/2019

ABSTRACT: Land cover/use changes specially the forest cover changes affect the local surface temperature (LST) of the earth. In this study, a combination of remote sensing and GIS techniques was used to scrutinize the interactions between LST anomalies and deforestation in Sardasht County, NW Iran. The land cover/use change layers of the study area were extracted from Landsat satellite imagery based on Binary Encoding classification and change detection technique. The radiometric correction analysis were done for each Landsat image to derive LST map layers. According to the results, a descending trend in forest cover with a total 2560 ha decline in area and an ascending trend of about 4 degrees rise in surface temperature values on both forest and non-forest areas were detected in the study area from 1984 to 2017. The temporal and spatial analysis yielded high rates of reverse temporal correlation (-0.81) between forest areas and LST anomalies while the correlation value of 0.76 was found for non-forest areas and LST. The regression analysis of the values confirmed the correlation results to be trustable at 99 percent. It was also found that the deforested areas of the study area correlate with the LST rise spatially with a very high correlation (0.98) from which a tangible interaction of the parameters can be inferred.

Keywords: *Iran, Land Surface Temperature, Sardasht, Zagros Forests*

1. Introduction

Land Surface Temperature (LST) is an important environmental parameter having valuable applications in different disciplines especially environmental sciences. Earth and environmental scientists take its benefit to monitor the interactions between surface temperature and climate conditions as there is a direct relation between climate change and LST variations. The variations in surface temperatures can also affect other important environmental phenomena like ice melting, drought, evapotranspiration, deforestation etc. Similar to human body temperature, the earth's surface temperature can be used as a diagnostic tool to detect and monitor arising challenges relating to rising surface temperatures. As LST changes impact soil moisture trends, some of the researchers have used this parameter to monitor and detect drought events in recent years (Karnieli et al ,2010; Son et al ,2012; Sruthi and Aslam ,2015; Arslan et al ,2016; Zhang et al ,2017; Gidy et al ,2018). Similarly, many researchers have recently focused on interactions between LST and landcover/landuse (LCLU) changes and confirmed that there is a clear correlation between surface temperature and land cover changes. For instance, Bakar et al (2016), applied three different indices to study the impacts of LCLU changes on LST and suggested that the NDVI, NDBI and MNDWI indices can be applied to monitoring land cover impacts on LST. Ding and Shi (2013), suggested that the development rate of Beijing Metropolis in China have led to the surface temperature increase of the city due to massive fast changes of land use. Amiri et al (2009) applied the Temperature Vegetation Index (TVI) to assess the interactions of LST and heat island of Tabriz city and recommended to use multi-temporal imageries to obtain better and more useful results. Xiao and Weng (2006) found that there is a strong agreement between surface temperature increases and built-up expansions. The direct implications of desertification and greenness loss on LST increase was confirmed by Entezari et al (2016). Manoharan et al (2009) analysed the deforestation rate and its impacts on regional temperatures and soil moisture and found very high correlation between NDVI, LST and soil moisture.
Sardasht is one of the green counties of Iran covered with Oak Forests which play a key role in social, economic and environmental sustainability of the western parts of the country. The combination of human interference in the nature of the region due to population growth in one hand and the widespread climate change impacts on the other hand, have put the health and existence of these resources in peril in recent decades. Since no study has been done in Iran West Forests regarding LST changes, the current study was designed to assess the status of land cover/use and surface temperature to see the now and then status of forest cover and LST values as well as the possible linkage between LST and deforestation/afforestation processes.

2. Materials and Methods

2.1. Study Area

Sardasht is one of the wooded counties of the country located between geographic coordinates of 45°13′48′′ to 45°42′00′′ E and 35°57′36′′ to 36°28′12′′ N in SW of West Azerbaijan province, NW of Iran (Figure1). It is a mountainous region with an average height of 1521m above sea level and is located on the green belt of oak forests in west of the country known as 'West Oak Forests' which sprawls from south to north. A moderate mountain climate dominates the local hydrometeorology of the area with an average precipitation of 724 mm/y and annual temperature of 13.3°C (Beygi Heidarlou et al., 2018). A concise information about the datasets are shown in Table 1. Remotely sensed images of different Landsat missions of NASA were downloaded from its online database (https://landsat.gsfc.nasa.gov/data/).

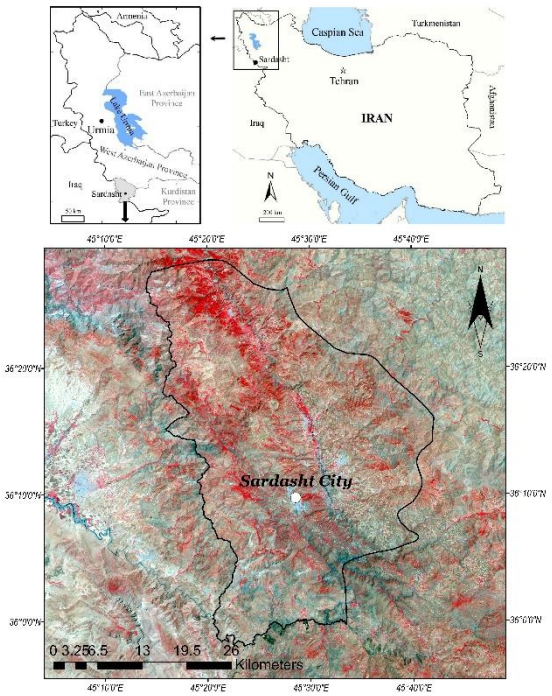

Figure 1. Geographic position of the study area (Landsat 8, 2016).

2.2. Digital Image Processing

2.2.1. Atmospheric Corrections

Satellite remote sensors are negatively influenced from atmospheric conditions (aerosols, clouds etc.) which lower the contrast of image features and harden the interpreter's task to detect real world features correctly. Since Landsat level-1 imageries are not corrected atmospherically, the images are first corrected for disturbing atmospheric conditions to pave the way for the commence of image classification procedure. In the current study, the Dark Object Subtraction (DOS) method was implemented for all the used imageries. DOS is an image-based method (Gilmore et al, 2015) which is used widely in remote sensing practices to eliminate the additive scattering (Cavez and Pet, 1988) impacts of the atmosphere from remote sensing data.

Table 1. Characteristics of the selected Multitemporal Landsat imageries for Sardasht county (path/row: 168/35).

Landsat Mission	5	5	5	5	7	5	5	7	8
Sensor	TM	TM	TM	TM	ETM+	TM	TM	ETM+	OLI
Acquisition Year	1984	1986	1993	1998	2002	2006	2010	2013	2017
Acquisition Date	27-Aug	02-Sep	19-Jul	19-Sep	06-Sep	09-Sep	19-Aug	17-Sep	23-Sep

2.2.2. Image Classification with Binary Encoding

As most raw data forms of satellite imagery restrict their scientific applications, image processing methods need to be implemented in order to extract useful information. Image classification is a well-known and routine step in any image processing procedure, in which each pixel or object is allocated to a real world feature on earth depending on the nature of the classification method (Pixel based or Object based). Its overall goal is to assign image pixels to land cover classes automatically (Kumar and Singh, 2013). Land cover/land use classification practices can be done by different strategies and algorithms provided by digital image processing tools (Cetin et al, 2004). The supervised classification method of Binary Encoding was applied in this study to do image classification.

The Binary Encoding (BE) is a standard classification technique for satellite imageries (Xie and Xiaohua (2012), in which the spectral data of images are put into 0s and 1s. The classification process in this approach is done based on a mean spectral threshold in a way that the pixels which fall below and above the threshold are classified as 0 and 1 respectively (ENVI Tutorials, 2012). Since it is mostly applied when there are just two target classes, in the present study the BE technique was used to derive two required land cover classes (Forest and Non Forest). To remove the annoying shadow effects on the imageries, the ratio transformation was implied for digitizing the training shapefile for classification. The results obtained from BE algorithm were enhanced using the appropriate NDVI values for each imagery. Eventually, the abnormal pixel values were removed by applying a Majority filter. This filter replaces the abnormal values by the most common value surrounding the cells.

Table 2. The accuracy assessment results of the classification for the study period

Year	Land Use / Land Cover ID									
	0	1	0	1	0	1	0	1		
	Producer's %		User's %		Commission Error		Omission Error		Overall Accuracy %	Kappa Coef
1984	100	100	100	100	0	0	0	0	100	1
1986	100	100	100	100	0	0	0	0	100	1
1993	90.17	92.77	92.87	90.07	9.83	7.23	7.13	9.93	91.45	0.82
1998	88.5	77.5	73.21	90.63	11.5	22.5	26.79	9.37	82	0.64
2002	97.22	90.57	92.11	96.64	7.89	3.36	2.78	9.43	94.10	0.88
2006	97.70	96.97	97.14	97.56	2.86	2.44	2.30	3.03	97.35	0.95
2010	95.03	97.47	97.73	94.48	2.27	5.52	4.97	2.53	96.17	0.92
2013	96.35	97.96	98.40	95.36	1.60	4.64	3.65	2.04	97.05	0.94
2017	97.81	96.15	96.76	97.40	3.24	2.60	2.19	3.85	97.05	0.94
	LCLU ID: Forest (1), Non Forest (0)									

2.3. Accuracy Assessment

The final step in any image classification approach is to check the accuracy of the classification to guarantee the trustworthiness of the results. The classification error matrix is one of the mostly used approaches in accuracy assessment practices in which the classified images are compared with ground truth points (Kumar and Singh, 2013). In this study the accuracy of the extracted LCLU map layers was assessed by applying ground-truth control points obtained from high-accuracy classification results of the previous studies and visual interpretation of remotely sensed imageries in order to achieve the highest possible precision. Overall accuracy, Kappa coefficient, user's and producer's accuracy values and commission and omission errors (Foody, 2002; Lu et al., 2004; Shooshtari and Gholamalifard, 2015) were computed (Table 2). The results of the assessment indicated that the classification accuracy has been satisfactory leading to the overall accuracy of more than 90% throughout the study period.

2.4. Retrieving Land Surface Temperature

Land surface temperature (LST) is a remotely sensed product demonstrating surface temperature of the earth where 'the received energy (heat and radiation) of the sun is absorbed, reflected or dispersed' (Anandababu et al, 2018). While some satellite sensors offer ready-to-use LST maps (at large scales), the usual and more applicable method for LST retrieval is to use thermal bands (TIR) of remotely sensed Landsat imageries. The mentioned steps below are the general approach of LST retrieval process which were followed in the current study to derive LST layers out of Landsat images for the study area. The specific parameters of thermal bands of different sensors used in the current study were received from metadata files offered with each sensor products by Landsat mission.

2.4.1. DN to Radiance Conversion

Digital numbers of thermal bands can be converted to the spectral radiances using the following equation (1). It depicts the outgoing energy radiated by the earth's surface sensed by each band at top of the atmosphere (Waters et al, 2002).

$$L_\lambda = \left(\frac{L_{Max} - L_{Min}}{(QCAL_{Max} - QCAL_{Min})}\right) \times (DN - QCAL_{Min}) + L_{Min} \quad (1)$$

Where DN is the digital number of each pixel, LMAX and LMIN are calibration constants, QCALMAX and QCALMIN are the highest and lowest range of values for rescaled radiance in DN. The units for Lλ are W/m2/sr/µm.

2.4.2. Radiance to Reflectance

Reflectance is defined as the ratio of incoming radiation to the outgoing radiation of the surface (Waters et al, 2002). It can be computed using the equation 2.

$$\rho_p = \frac{\pi \times L_\lambda \times d^2}{ESUN_\lambda \times \cos\theta_s} \quad (2)$$

Where ρ_p is reflectance (Unitless), L_λ is spectral radiance, d is Earth-Sun distance in astronomical units, $ESUN_\lambda$ is Mean solar exoatmospheric irradiances, and θ_s is solar zenith angle in degrees.

2.4.3. Reflectance to At-Satellite Temperature

The following equation is used to convert the radiance to temperature.

$$T = \frac{K_2}{\ln(\frac{K_1}{L_\lambda} + 1)} \quad (3)$$

Where T is effective at-satellite temperature (Kelvin), K1 and K2 are constants for Landsat images (Markham and Barker, 1987).

2.4.4. At-Satellite Temperature to Surface Temperature

At the final step, desired LST can be calculated using the following equation (Artis and Carnahan, 1982).

$$LST = \frac{BT}{1 + (\lambda \times \frac{BT}{P}) \ln(e)} \quad (4)$$

Where BT is at satellite brightness temperature, λ is the wavelength of emitted radiance, P=h×c/s (1.438×10-2mk) P=14380, h= Planck's constant (6.626×10-34 Js), s=Boltzmann Constant (1.38×10-23 J/K), c= Velocity of light (2.998x10-8 m/s).

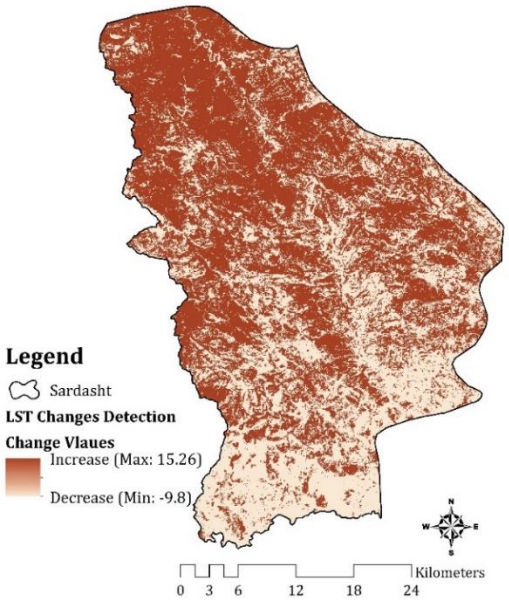

Figure 2. The visual fluctuations of LST values in the study area.

3. Results and Discussion

3.1. LST Anomalies

Calculating the required LST maps, the temporal variations of the environment temperature on each land cover class of the study area were extracted (Table 3). The results shows that while a slight wax and wane is seen in the values, the total trend of LST measures is ascending for both the land covers with an almost the same changes

(4.0 degrees in non-forest and 3.9 degrees in forest class) through the study period.
The change detection map of LST also illustrates the spatial spread of the LST changes throughout the area. Figure 2, shows the total LST variations from 1984 to 2017 for the study area. While the max and min variations are 15 and -9.8 degrees respectively, the mean values correspond the temporal trends as mentioned before.

Table 3. The areal-mean LST variations regarding each LCLU category

Land Cover	LST								
	1984	1986	1993	1998	2002	2006	2010	2013	2017
Non Forest	37.99	37.22	36.37	34.71	37.09	40.86	41.65	39.62	41.90
Forest	33.71	33.27	32.18	30.29	33.68	36.33	37.67	35.45	37.60

3.2. Land Cover/Use Changes

The statistics derived from LCLU map layers (Table 4) shows the temporal changes in Forest and Non-Forest areas during time. As expected, the trends are ascending for non-forest and descending for forest areas (Figure 4) with a high correlation value (about 98.5% for each land cover). These changes have been pictured for better understanding in figure 3. The results indicate about 7700 hectares decline in forest area in the last three decades, which corresponds to 5.6% of the total area of the region. On the other hand the destructed forest has been transformed into the other land uses, which was seen from increased non-forest area.
To examine the spatial changes occurred in forest cover of the region, the change detection map was derived (Figure 3). The figure represents the total status of deforestation and afforestation process in the region during the last three decades. According to the change detection information obtained for the period 1984-2017, about 9700 ha forest cover change was detected from which 7700 ha was defined as forest loss and 2000 ha as forest gain. About 128000 ha of the study area was detected to suffer no change during the same period.

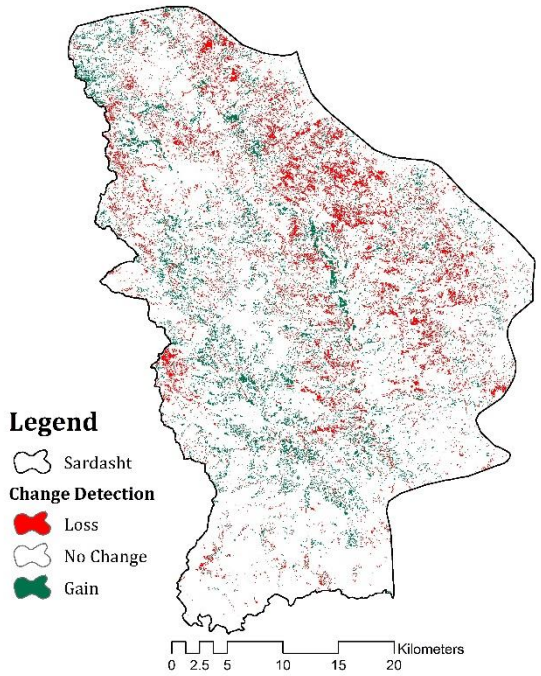

Figure 3. The spatial illustration of forest cover changes during the study period.

Table 4. The LCLU changes for each category from 1984 to 2017.

Land Cover	Area (km^2)								
	1984	1986	1993	1998	2002	2006	2010	2013	2017
Non Forest	1009	1027	962	809	1024	1014	1033	1029	1086
Forest	372	354	420	573	358	367	349	353	295

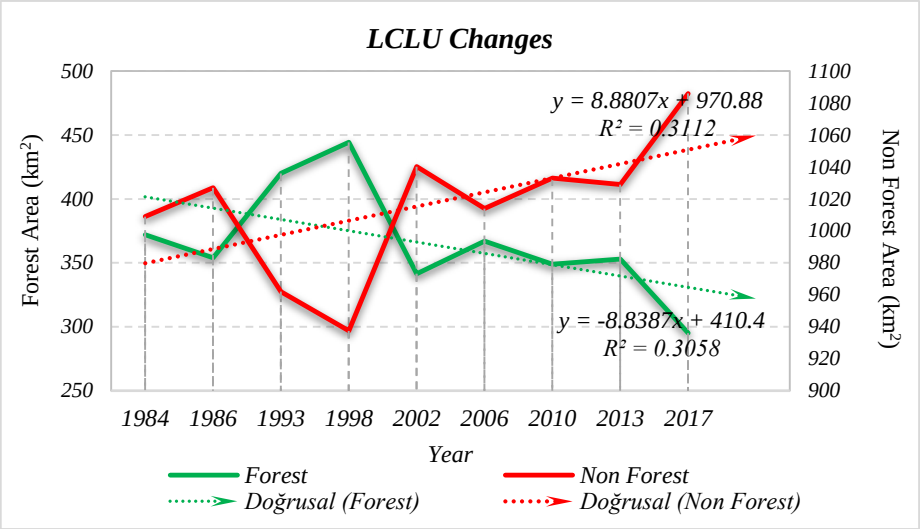

Figure 4. The temporal changes of land cover/use values

3.3. Forest/Non-Forest Cover Changes Impacts on LST Variations

The wooded areas have a great potentiality to alleviate the harsh climatic conditions interacting with the sun radiations thus providing shadow to lower the temperatures. Theoretically, the forest degradation would have reverse impact on temperature values (either air or surface temperature) so that the more deforestation occurs, the more the temperature rises up. To study this relation in Sardasht County, the calculated measures were compared in a statistical manner. Comparing the two change detection maps (LST and LCLU) a very high spatial correlation coefficient of 0.98 was detected between forest loss and LST increase areas which confirms the found relation spatially. On the other hand the high correlation (98.2%) was detected for forest gain areas with LST changes.

To reveal the LST feedbacks to the current forest and non-forest cover change information, the temporal trend lines were drawn as shown in Figures 5 and 6 respectively. Accordingly, though the trend lines of forest change mimic each other in some short periods (1984 and 2006), the relation between deforestation and LST variations seems logical for the remaining periods with a total temporal correlation of -0.81 which is meaningful at 0.01 significance level where the destructed forest leads to increasing temperatures through time. On the other hand the trends in non-forest areas follows the LST trends through the study period indicating the positive relation between changing non-forested areas and LST values with an estimated correction of 0.71. Table 5 shows the correlation statistics of forest/non-forest temporal changes and LST variations during the study period.

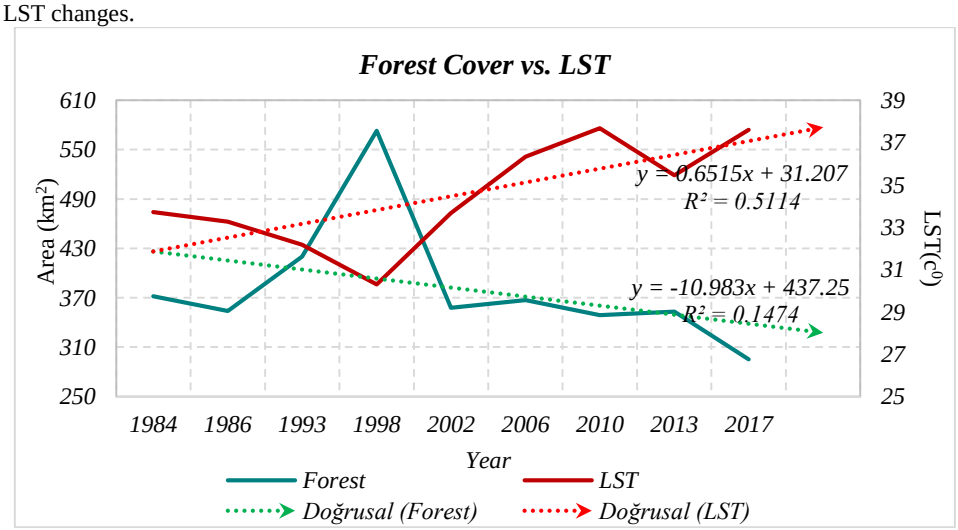

Figure 5. The temporal interactions of forest and LST changes

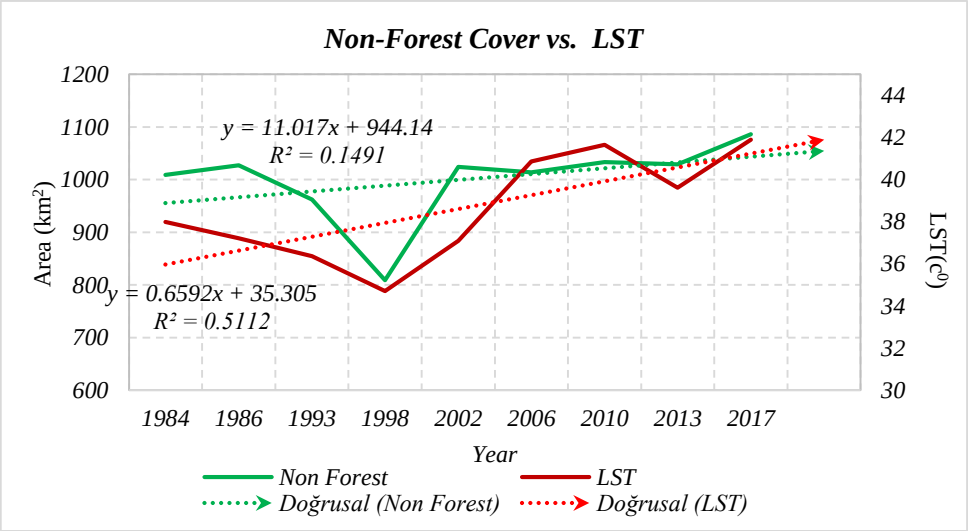

Figure 6. The temporal interactions of non-forest and LST changes.

Table 5. The correlation rate and linear regression function of LCLU and LST changes

	Regression Function	R	Significance level
Forest/ LST	Y= 44.26 - 0.0256×X	-0.81	0.01
Non Forest/ LST	Y= 14.15 + 0.0245×X	0.76	0.01

Overall, the results indicated that the study area has suffered severe degradation process from 1984 to 2017 loosing 2560 ha of its forest coverage. The temporal results suggested that a rational trend obtains between deteriorating process of LCLU changes and LST fluctuations in both forest and non-forest classes. The decreasing forest cover was associated with increasing LST in cleared out areas with a mean value of 3.8^{0}C. On the other hand, 4^{0}C of mean LST increase was found in the increasing non-forest areas. The spatial comparison of the changes also revealed that the total changes in forest cover (deforestation and afforestation) and LST trends go hand in hand closely with a 98.5% and 98.2% of correlation for forest loss and forest gain points with LST changes respectively which proves the direct negative contribution of forest change to increasing surface temperatures.

4. Conclusion

The main goal of the current study was to analyze the impacts of deforestation on land surface temperature variations. Since some of the important environmental phenomena can be inferred from temperature anomalies of the earth's surface, monitoring LST changes seems to have a pivotal role in any environmental conservation policy. In this study the temporal as well as spatial changes of land cover/use and surface temperatures were analyzed to incorporate the results in assessment of the possible expected impacts of the changing LCLU on LST variations. As a concluding results for this study it can be said that deforestation process as an outcome of human interferences in the nature have had the most tangible implications for the changing temperature values of the environment of Sardasht. The LST anomalies appeared to have a close relation with deforestation and afforestation processes so it is suggested that LST monitoring can be used as a diagnostic mean to study the health and status of wooded areas to make the decision makers much more able to guard these natural resources.

References

Amiri R., Weng Q., Alimohammadi A. and Alavipanah S.K (2009). Spatial–temporal dynamics of land surface temperature in relation to fractional vegetation cover and land use/cover in the Tabriz urban area, Iran. Remote sensing of environment, 113(12), pp.2606-2617.

Anandababu D., Purushothaman BM. and Babu SS (2018). Estimation of Land Surface Temperature using LANDSAT 8 Data. International Journal of Advance Research, Ideas and Innovations in Technology. 4(2):177-86.

Arslan M., Zahid R.and Ghauri B (2016). Assessing the occurrence of drought based on NDVI, LST and rainfall pattern during 2010–2014. Geoscience and Remote Sensing Symposium (IGARSS), 2016 IEEE International (pp. 4233-4236). IEEE.

Artis D.A. and Carnahan W.H (1982). Survey of emissivity variability in thermography of urban areas. Remote Sensing of Environment, 12(4), pp.313-329.

Bakar S.B.A., Pradhan B., Lay U.S. and Abdullahi S (2016). Spatial assessment of land surface temperature and land use/land cover in Langkawi Island. In IOP Conference Series: Earth and Environmental Science.Vol. 37, No. 1, p. 012064.

Beygi Heidarlou H., Banj Shafiei A., Erfanian M., Tayyebi. and Alijanpour A (2015). Detection of land cover changes in Sardasht during time period of 1993 to 2016. The International Conference on Natural Resources

Management in Developing Countries, Iran, Tehran, 25 Feb. 2015.

Cetin M., Kavzoglu T. and Musaoglu N (2004). Classification of multi-spectral, multi-temporal and multi-sensor images using principal components analysis and artificial neural networks: Beykoz case. In Proceedings XXth International Society for Photogrammetry and Remote Sensing-Congress, pp. 12-23.

Chavez Jr. and Pat S (1988). An improved dark-object subtraction technique for atmospheric scattering correction of multispectral data. Remote sensing of environment 24, no. 3: 459-479.

Ding H. and Shi W (2013). Land-use/land-cover change and its influence on surface temperature: a case study in Beijing City. International Journal of Remote Sensing, 34(15), pp.5503-5517.

Entezari A., Ahmadi A., Aliabadi K., Khosravian M. and Ebrahimi M (2016). Monitoring Land Surface Temperature and Evaluating Change Detection Land Use (Case Study:Parishan Lake Basin), Hydrogeomorphology, v2[8],113-139.

Foody GM. (2002). Status of land cover classification accuracy assessment Remote Sensing of Environment 80:185-201 doi:10.1016/S0034-4257(01)00295-4.

Gidey E., Dikinya O., Sebego R., Segosebe E. and Zenebe A (2018). Analysis of the long-term agricultural drought onset, cessation, duration, frequency, severity and spatial extent using Vegetation Health Index (VHI) in Raya and its environs, Northern Ethiopia. Environmental Systems Research, 7(1), p.13.

Gilmore S., Saleem A. and Dewan A. (2015). Effectiveness of DOS (Dark-Object Subtraction) method and water index techniques to map wetlands in a rapidly urbanising megacity with Landsat 8 data. Research@ Locate'15, pp.100-108.

Karnieli A., Agam N., Pinker R.T., Anderson M., Imhoff M.L., Gutman G.G., Panov N. and Goldberg A. (2010). Use of NDVI and land surface temperature for drought assessment: Merits and limitations. Journal of climate, 23(3), pp.618-633.

Kumar M. and Singh R.K. (2013). Digital Image Processing of Remotely Sensed Satellite Images for Information Extraction. In Conference on Advances in Communication and Control Systems (CAC2S).

Lu D., Mausel P., Brondizio E. and Moran E. (2004). Change detection techniques. International journal of remote sensing. 1; 25(12):2365-401.

Manoharan V.S., Welch R.M. and Lawton R.O. (2009). Impact of deforestation on regional surface temperatures and moisture in the Maya lowlands of Guatemala. Geophysical Research Letters, 36(21).

Markham B.L. and Barker J.L. (1987). Thematic Mapper bandpass solar exoatmospheric irradiances. International Journal of remote sensing 8, no. 3 517-523.

Research Systems, Inc. ENVI tutorials. Research Systems, September, 2001 Edition. gers.uprm.edu/geol6225/pdfs/envy_tutorial.pdf (Accessed 05.09.2018).

Shooshtari SJ. and Gholamalifard M. (2015). Scenario-based land cover change modeling and its implications for landscape pattern analysis in the Neka Watershed, Iran Remote Sensing Applications: Society and Environment 1:1-19

Son N.T., Chen C.F., Chen C.R., Chang L.Y. and Minh V.Q (2012). Monitoring agricultural drought in the Lower Mekong Basin using MODIS NDVI and land surface temperature data. International Journal of Applied Earth Observation and Geoinformation, 18, pp.417-427.

Sruthi S. and Aslam M.M. (2015). Agricultural drought analysis using the NDVI and land surface temperature data; a case study of Raichur district. Aquatic Procedia, 4, pp.1258-1264.

Waters R., Allen R., Bastiaanssen W., Tasumi M. and Trezza R. (2002). Surface energy balance algorithms for land, Idaho implementation, advanced training and user's manual. NASA, USA.

Xiao H. and Weng Q. (2007). The impact of land use and land cover changes on land surface temperature in a karst area of China. Journal of environmental management, 85(1), pp.245-257.

Xie H. and Xiaohua T. (2012). An inproved binary encoding algorithm for classification of hyperspectral images. In Hyperspectral Image and Signal Processing (WHISPERS), 2012 4th Workshop on, pp. 1-4. IEEE.

Zhang X., Yamaguchi Y., Li F., He B. and Chen Y. (2017). Assessing the impacts of the 2009/2010 drought on vegetation indices, normalized difference water index, and land surface temperature in Southwestern China. Advances in Meteorology. Volume 2017, Article ID 6837493, 9 pages.